

Fluorometric sensing of Hg²⁺ ions in aqueous medium by nano-aggregates of a tripodal receptor†

Cite this: *Org. Biomol. Chem.*, 2014, **12**, 2302

Ajнеш Singh,^{‡a} Simanpreet Kaur,^{‡b} Narinder Singh^{*a} and Navneet Kaur^{*b}

Two new tripodal receptors (**1**–**2**) have been synthesized and characterized by various spectroscopic techniques. The nano-aggregates of **1** and **2** (**N1** and **N2**) have been prepared by a re-precipitation method in aqueous medium and have shown different photo-physical properties. Nano-aggregates of **1** (**N1**) can selectively recognize Hg²⁺ in aqueous medium in the presence of other metal ions with enhancement in fluorescent intensity. The response was linearly proportional to the concentration of Hg²⁺ in the range 0–10 μM with a detection limit of 2.4 nM. The mechanism of selective binding of Hg²⁺ by **N1** has also been supported by theoretical studies. To the best of our knowledge, this work represents the first report on substituted thiourea based nano-aggregates for nano-molar detection of mercury in aqueous medium.

Received 6th November 2013,
Accepted 19th January 2014

DOI: 10.1039/c3ob42200c

www.rsc.org/obc

Introduction

In recent years, a lot of effort has been devoted into the design and synthesis of simple, cheap and efficient molecules/receptors for sensing and recognition of biologically and environmentally important metal ions/anions.^{1–9} Receptor molecules, which are capable of selective recognition and sensing of heavy and transition metal ions, are of great importance due to the significance of metal ions in the cellular world or noxious effects on the environment and human health. Mercury is one such heavy metal that has attracted considerable attention from the time of the Minamata disaster to the present time. Mercury in the form of Hg²⁺ ions is a carcinogenic material with a high degree of cellular toxicity. Even a low concentration of about 5 ppb can cause significant harmful effects. The accumulation of Hg²⁺ ions is found to be responsible for many serious diseases such as prenatal brain damage, mitosis impairment and nervous system related disorders.^{10–13} Out of the reported methods for detection of Hg²⁺, colorimetric and fluorometric methods offer numerous advantages in terms of high selectivity, sensitivity, time

efficiency and direct visual detection.^{14–28} Thus, much effort has been devoted in the fabrication of new sensitive and selective methods for determination of toxic mercury.

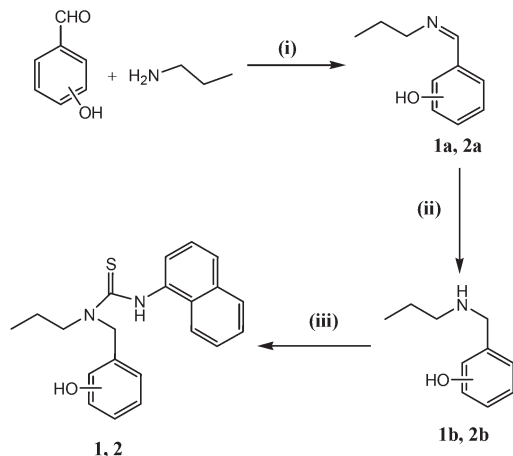
Recently, number of fluorescent probes for Hg²⁺ detection have been reported,^{14–28} where the majority of the probes work with a “fluorescence off” (fluorescence quenching) and “fluorescence on” (fluorescence enhancement) mechanism. Moreover, these probes work efficiently in organic solvents or mixed solution of organic solvent–water which limits their application in biological and environmental samples. Thus, receptors which can work in aqueous medium are of great interest. Conventional organic probes show high fluorescence in dilute solutions; however, when dispersed in aqueous medium this leads to weakening or even quenching of intensity. But recent advances in nanoparticles/aggregates based chemosensors have equipped the supra-molecular chemists with a new strategy. Here in, organic molecules dispersed in aqueous medium in the form of nano-aggregates can be utilized as chemosensors.^{29–33} In the present studies, we have synthesized two new tripodal receptors with a naphthyl unit as a hydrophobic fluorophore and a soft sulphur centre as donor for heavy metal detection. Interesting photo-physical properties of receptors have been observed in pure acetonitrile solution and as nano-aggregates dispersed in aqueous medium. Here, we have utilized a new strategy where nano-aggregates of organic molecules dispersed in aqueous medium were utilized as alternative sensing materials for metal ions,³³ in which receptor molecules dispersed in pure water medium again rearranges themselves in a more static conformation through multivalent interactions, resulting in an intense emission in

^aDepartment of Chemistry, Indian Institute of Technology Ropar (IIT Ropar), Rupnagar, Punjab 140001, India. E-mail: nsingh@iitrpr.ac.in; Tel: +91-1881242176

^bCentre for Nanoscience and Nanotechnology (UIEAST), Punjab University, Chandigarh, 160014, India. E-mail: navneetkaur@pu.ac.in; Tel: +91-1722534464

†Electronic supplementary information (ESI) available: Experimental details, UV-vis absorption spectra, fluorescence spectra, NMR spectra, mass spectra. See DOI: 10.1039/c3ob42200c

‡Both authors have contributed equally.



Scheme 1 Synthetic procedure employed for the syntheses of compounds 1–2; 1 = *ortho* derivative, 2 = *para* derivative; (i) MeOH, rt; (ii) MeOH, NaBH₄, rt; (iii) CHCl₃ (dry), 1-naphthyl isothiocyanate, reflux (4 h).

the presence of metal ions. This strategy offers an interesting method for the sensing of metal ions in pure aqueous medium with a “fluorescence on” mechanism.

This paper reports the synthesis of two tripodal receptors (1–2) and the preparation of their nano-aggregates (N1–2) in aqueous medium by a re-precipitation method.³⁴ These aggregates were further employed as potential sensors for Hg²⁺ in an almost pure aqueous system. The effect of the position of substituents on aggregation behaviour was also studied in detail.

Results and discussion

Syntheses

The receptors 1–2 were synthesized by the condensation of *n*-propylamine and 2/4-hydroxybenzaldehyde, followed by reduction with NaBH₄ and further reaction of the reduced product with 1-naphthyl isothiocyanate (Scheme 1). The compounds 1–2 were fully characterized with CHN analysis, ¹H and ¹³C NMR, FT IR and mass spectroscopy (Fig. S1–S8, ESI†).

Effect of water content on photo-physical properties

The UV-Vis spectra of receptors 1 and 2 were recorded with 10 μM concentration in acetonitrile and showed two peaks in the regions 220–230 nm and 280–285 nm; these peaks are attributed to π–π* transitions. As the solvent system was changed from acetonitrile to water, the bathochromic shift of 25 nm (Fig. 1, peak shifted from 285 nm to 310 nm) with decrease in absorbance was observed in the case of compound 1; while no significant effect was noticed on the absorption profile of compound 2 (Fig. 1). Similarly, fluorescence spectra recorded in acetonitrile/aqueous medium have shown unique fluorescence profiles for each compound (Fig. 2). In compound 1, change of solvent system has shown two significant effects on the emission profile; a red shift and enhancement in the

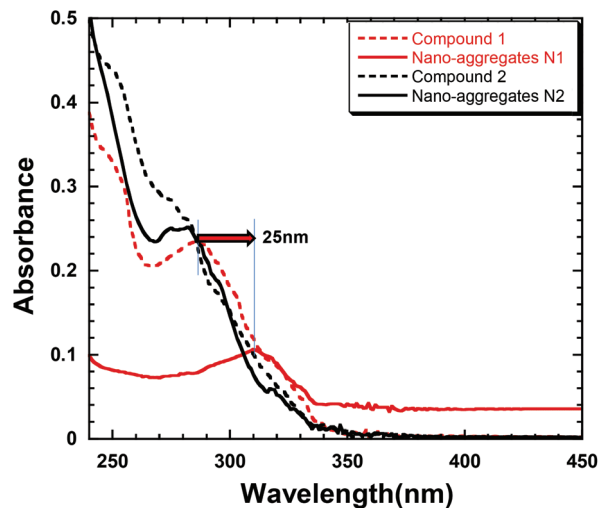


Fig. 1 Absorption spectra of compounds 1 (10 μM) and 2 (10 μM) in acetonitrile and nano-aggregates N1 (10 μM) and N2 (10 μM) in water.

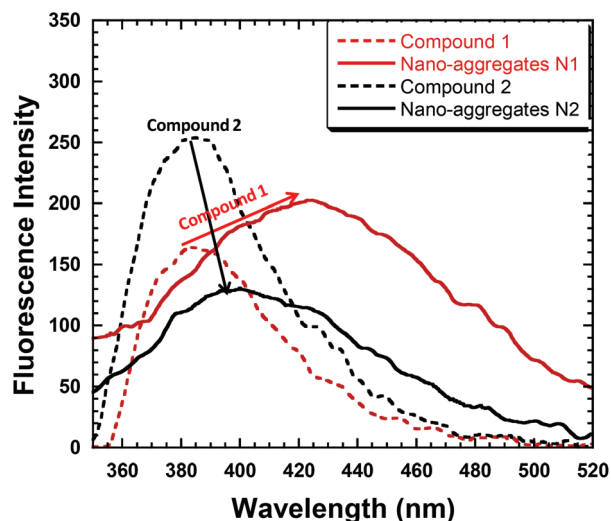


Fig. 2 Emission spectra of compounds 1 (10 μM) and 2 (10 μM) in acetonitrile and nano-aggregates N1 (10 μM) and N2 (10 μM) in water.

fluorescence intensity of the receptor as shown in Fig. 2. This change in photo-physical properties can be explained on the basis of formation of nano-aggregates with change in solvent system. The enhancement in fluorescent emission is due to the restriction of intramolecular rotations that prevent non-radiative decay for fluorescence quenching and responsible for the high fluorescence efficiency with bathochromic shift.³⁵ In compound 2, a totally opposite phenomenon was observed (Fig. 2). In this case, an increased water content led to formation of aggregates, which induces a decrease in the fluorescence intensity, or this effect can be referred to as “aggregation caused quenching” (ACQ).^{36,37} A possible reason behind this ACQ in aggregates of 2, could be the strong π–π stacking interactions between the *p*-phenolic and naphthyl rings. These interactions prompt the formation of such

detrimental species as excimers, thus leading to the observed ACQ effect.

The effect of water content on the formation of nano-aggregates was also studied by varying the water content from 0–100%. It was observed that nano-aggregates started forming only when the water content was 80% or more in the mixture and best results were obtained with 100% water (Fig. S9†). Also, formation of nano-aggregates is dependent on the time given during the sonication. It was observed that nano-aggregates of homogenous size were obtained only after 10 minutes of sonication, if the solution was sonicated for less time only aggregates of large size with non-homogenous distribution of particles were formed.

Effect of concentration of receptor on the aggregation

The effect of the concentration of the receptor on the formation of nano-aggregates was monitored by recording their absorption and emission spectra at different concentrations (10, 20, 50 and 100 μM , Fig. 3). Also, the change in size was also monitored with the help of DLS studies (Fig. 4A). DLS analysis provides an estimate of the particle size, which showed that the particle size increased with an increase in amount of 1 and 2 used (Fig. 4B). The controlled precipitation along with non-polar interactions among larger amounts of compounds may contribute to the generation of larger sized particles. The larger particles systematically produce prominent absorbance peaks (Fig. 3A & B) and thus depict the involvement of similar arrangements in the aggregate formation. Similarly, an enhanced fluorescence emission was observed with increase in size (Fig. 3C and D).

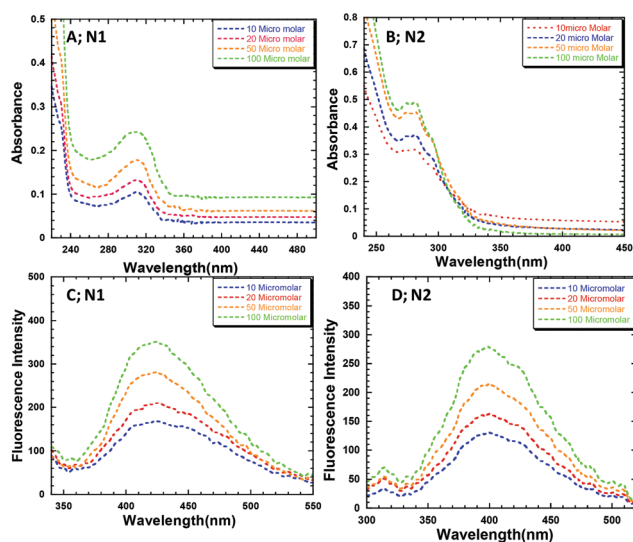


Fig. 3 (A) Changes in the UV-Vis profile of nano-aggregates N1 at different concentrations (10, 20, 50 and 100 μM); (B) changes in the UV-Vis profile of nano-aggregates N2 at different concentrations (10, 20, 50 and 100 μM); (C) changes in the emission profile of nano-aggregates N1 at different concentrations (10, 20, 50 and 100 μM) and (D) changes in the emission profile of nano-aggregates N2 at different concentrations (10, 20, 50 and 100 μM).

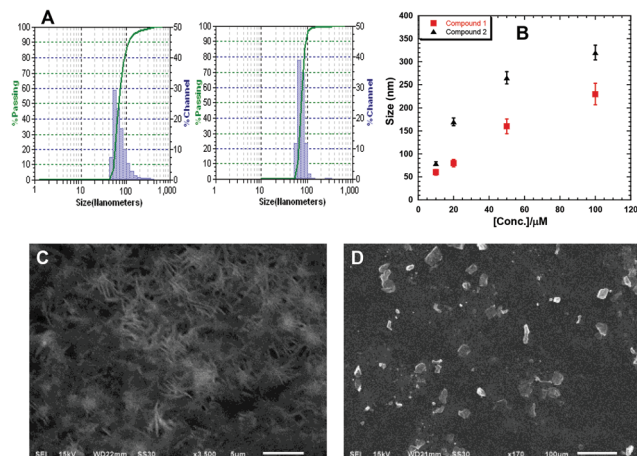


Fig. 4 (A) DLS histograms of N1 (66 nm) and N2 (79 nm) at concentration 10 μM ; (B) plot showing the variation in size of aggregates as a function of concentration of compound in aqueous medium; (C & D) SEM images of N1 and N2, respectively.

The figures do not show any shift in the absorbance or fluorescence maximum with size, which can be attributed to a similar kind of arrangement of ligand molecules in nano-aggregates of different dimensions as well as to their uniform dispersions in aqueous phase. When SEM images were recorded for nano-aggregates N1 and N2, different type of morphologies of the aggregated particles were observed as shown in Fig. 4C and D.

Recognition studies

Nano-aggregates N1. To evaluate the cation recognition behaviour of nano-aggregates of receptor 1 (N1) dispersed in aqueous medium, changes in the emission profile (excited at 310 nm) were monitored on addition of different metal nitrate salts (50 μM) such as Li^+ , Na^+ , K^+ , Cs^+ , Mg^{2+} , Ca^{2+} , Ba^{2+} , Sr^{2+} , Al^{3+} , Cr^{3+} , Mn^{2+} , Fe^{3+} , Co^{2+} , Cu^{2+} , Zn^{2+} , Ag^+ , Pb^{2+} , Cd^{2+} and Hg^{2+} to a fixed concentration (10 μM) of nano-aggregates N1 (Fig. 5A). The emission profile of nano-aggregates N1 have not shown any significant change with most of the metal ions tested; however, addition of Hg^{2+} has produced an enhancement in the fluorescence intensity (approx. four fold) with formation of a new peak centred at 415 nm. This enhancement in the fluorescence intensity may be attributed to the interaction of Hg^{2+} ions with ligand molecules which led to the arrangement of ligand molecules in a more static conformation through multivalent interactions, resulting in an intense emission in presence of metal ions.³³ The enhancement in fluorescence intensity with a negligible shift in the emission maxima might be due to the inhibition of the photo-induced electron transfer (PET) mechanism.³⁸ To investigate the binding behaviour of nano-aggregates N1 and Hg^{2+} ions, a titration was performed in which Hg^{2+} ions were added in small aliquots to a fixed concentration of the host solution (10 μM). The successive additions of Hg^{2+} ion (0–50 μM) to the host solution have been consistent with changes observed in the metal binding tests. The increase in the amount of Hg^{2+}

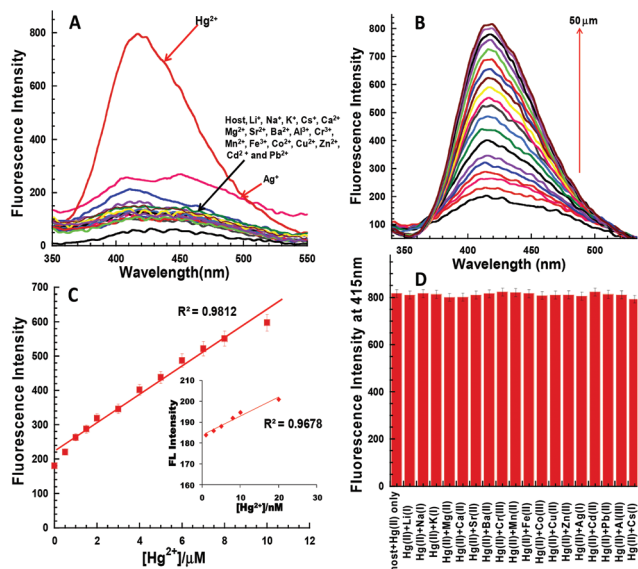


Fig. 5 (A) Changes in emission profile of nano-aggregates **N1** (10 μM) in water upon addition of 50 μM of a particular metal nitrate salts; (B) changes in emission profile of nano-aggregates **N1** (10 μM) upon successive addition of Hg^{2+} (0–50 μM); (C) linear regression graph between concentration of mercury ion added (0–10 μM) and increase in fluorescence intensity of nano-aggregates **N1** (25 μM), Inset; linear regression plot of nano-aggregates **N1** (10 μM) and Hg^{2+} added in 0–20 nM range; (D) influence of other metal ions on the Hg^{2+} based changes in the emission profile of nano-aggregates **N1**.

ion added to host solution is directly proportional to the increase in the intensity of the band at 415 nm (Fig. 5B). Titration showed a good linearity in a range of 0–10 μM concentration of mercury (Fig. 5C). Using these titration data, nano-aggregates **N1** can detect Hg^{2+} ion in the solution up to 2.4 nM level (3σ method, inset Fig. 5C, S10 \dagger).³⁹ To check the selectivity of nano-aggregates for Hg^{2+} ions, competitive metal binding experiments were also performed to estimate Hg^{2+} (50 μM) in the presence of any of Li^+ , Na^+ , K^+ , Cs^+ , Mg^{2+} , Ca^{2+} , Ba^{2+} , Sr^{2+} , Al^{3+} , Cr^{3+} , Mn^{2+} , Fe^{3+} , Co^{2+} , Cu^{2+} , Zn^{2+} , Ag^+ , Pb^{2+} and Cd^{2+} (50 μM).

As shown in Fig. 5D, no significant variation in the fluorescence intensity is observed by comparing the profile with and without the other metal ions, and this indicates that nano-aggregates **N1** have a high selectivity for Hg^{2+} . The anion binding tests of nano-aggregates of **1** with variety of anions (F^- , Cl^- , Br^- , I^- , PO_4^{3-} , ClO_4^- , HSO_4^- , CN^- and CH_3COO^-) have not shown any significant changes in emission spectra (Fig. S11 \dagger).

Nano-aggregates N2. The cation recognition behavior of nano-aggregates **N2** was evaluated from changes in the fluorescence spectra upon addition of a particular metal salt (50 μM) to a solution of nano-aggregates **N2** in aqueous medium (10 μM). The emission profiles of nano-aggregates **N2** in the presence of Hg^{2+} and Mn^{2+} ions were different, with increase in fluorescence intensity of the band at 380 nm and formation of a new band at 465 nm in the case of Hg^{2+} and Mn^{2+} , respectively (Fig. 6A). Also, a slight increase in the

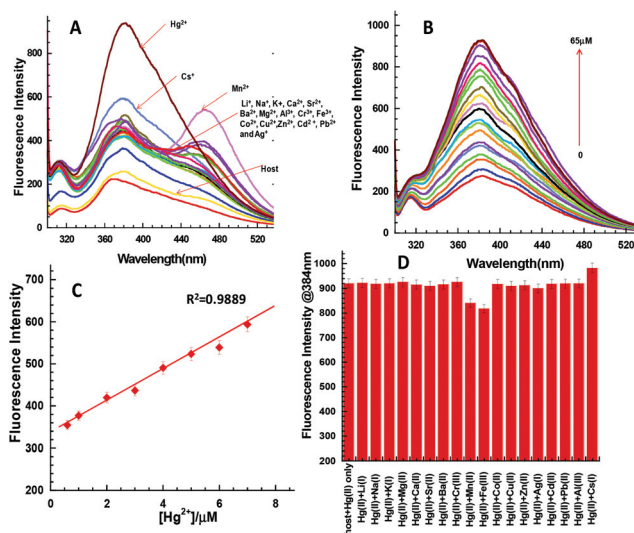


Fig. 6 (A) Changes in emission profile of nano-aggregates **N2** (10 μM) in aqueous medium upon addition of 50 μM of a particular metal nitrate salt; (B) changes in emission profile of nano-aggregates **N2** (10 μM) upon successive addition of Hg^{2+} (0–65 μM); (C) linear regression graph between concentration of mercury ion added and increase in fluorescence intensity; (D) influence of other metal ions on the Hg^{2+} based changes in the emission profile of nano-aggregates **N2**.

emission band at 380 nm is also observed on addition of Cs^+ ions. However, addition of Hg^{2+} ion have produced more significant changes than other ions, therefore we have only utilized nano-aggregates **N2** as sensors for mercury ions. To gain more insight about the sensor activity of nano-aggregates **N2** for Hg^{2+} a titration (Fig. 6B) was performed by taking 10 μM of nano-aggregates **N2** with successive addition of Hg^{2+} (0–65 μM) in aqueous medium. Successive addition of Hg^{2+} to the solution of nano-aggregates **N2** led to continuous enhancement in the fluorescence intensity at 380 nm. The titrations showed a good linearity in a range of 0.6 μM –7.0 μM concentration (Fig. 6C) of mercury. Competitive metal binding experiments were also performed to estimate Hg^{2+} (50 μM) in the presence of any of Li^+ , Na^+ , K^+ , Cs^+ , Mg^{2+} , Ca^{2+} , Ba^{2+} , Sr^{2+} , Al^{3+} , Cr^{3+} , Mn^{2+} , Fe^{3+} , Zn^{2+} , Co^{2+} , Cu^{2+} , Ag^+ , Pb^{2+} and Cd^{2+} (50 μM) to check the practical applicability of nano-aggregates **N2** as sensor for Hg^{2+} (Fig. 6D) ions. As shown in Fig. 6D, a slight interference was observed with metal ions such as Mn^{2+} and Cs^+ which means that nano-aggregates **N2** are not as selective for Hg^{2+} ions as nano-aggregates **N1**. Anion binding tests of nano-aggregates **N2** with a variety of anions (F^- , Cl^- , Br^- , I^- , PO_4^{3-} , ClO_4^- , HSO_4^- , CN^- and CH_3COO^-) have not shown any significant changes in emission spectra. The response is similar to that of nano-aggregates **N1** and is shown in Fig. S12 \dagger .

pH effect, salt effect and response time

To check the utility of nano-aggregates, the emission spectra response of nano-aggregates **N1** at different pH values in the absence and presence of Hg^{2+} was monitored. The fluorescence intensity decreased as the pH of the solution was

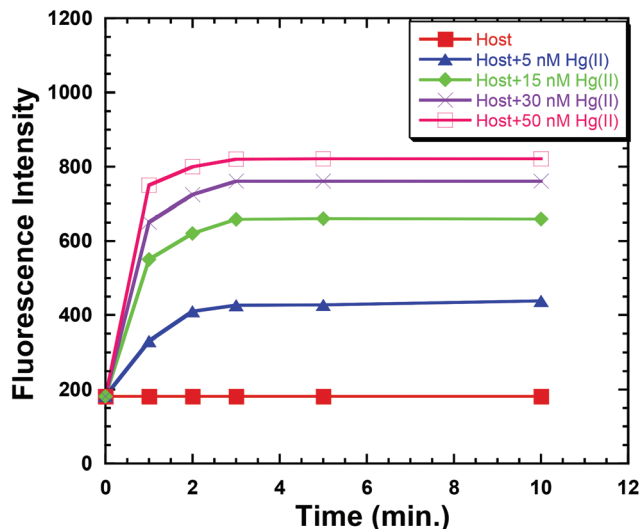


Fig. 7 Plot of fluorescence intensity of nano-aggregates **N1** and Hg^{2+} at different concentrations (5, 15, 30 and 50 μM) as a function of time (minutes).

changed from neutral to acidic, which was likely due to formation of large aggregates due to agglomeration. No change in the emission spectra of nano-aggregates **N1** was observed in the pH range 6–13 (Fig. S13[†]). Therefore, nano-aggregates **N1** were favourable for application in a wide pH range (3–13). Further, the response of nano-aggregates **N1** for Hg^{2+} was also studied as a function of time by monitoring changes in the fluorescence spectra. In a typical experiment, different concentrations of Hg^{2+} (5, 15, 30 and 50 μM) were added to solutions of fixed concentration (10 μM) of nano-aggregates **N1** and fluorescence spectra were recorded at small intervals of time (Fig. 7). The results showed that, Hg^{2+} ions interact with nano-aggregates **N1** within the first 3 minutes and after this no change in the fluorescence intensity was observed with increased time up to 15 minutes. Perturbation of high ionic strength was ruled out by comparison of fluorescence spectra of nano-aggregates **N1** (recorded with 25 μM concentration of host in H_2O) with the respective fluorescence spectrum recorded upon addition of 0–200 equiv. of tetrabutyl ammonium nitrate under the same concentration of host and solvent system (Fig. S14[†]).

NMR titration

In an effort to understand the binding behaviour of Hg^{2+} ions with **1**, ^1H NMR titration was performed between compound **1** and Hg^{2+} ion in the form of nitrate salt in $\text{DMSO}-d_6$. The NMR titration was performed by varying the equivalent of Hg^{2+} with respect to compound **1** (Fig. 8). An equivalent of 0.25 induces a broadening and shift of $\Delta\delta = 0.04$ ppm in the signal of $-\text{OH}$ (9.38 ppm). At one equivalent, the $-\text{OH}$ signal merged into the $-\text{NH}$ signal with total downfield shift of $\Delta\delta = 0.5$. Also, the benzylic protons (CH_2) were shifted upfield from 5.06 to 4.98 ppm. The downfield shift in the $-\text{NH}$ signal (9.75 to 9.89 ppm) indicated the coordination of Hg^{2+} with sulphur.

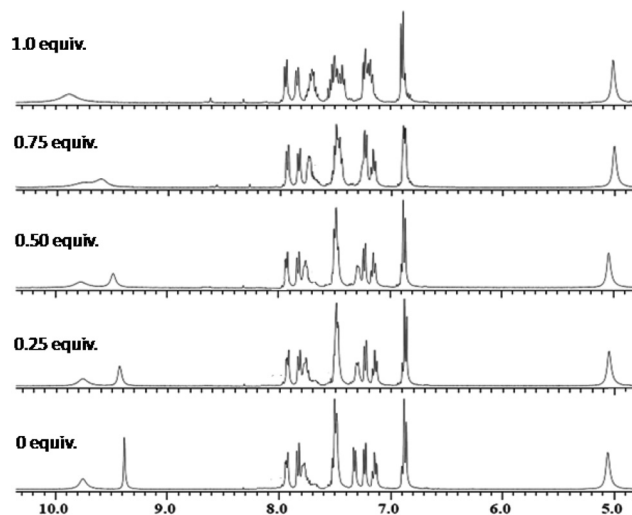


Fig. 8 ^1H NMR titration of compound **1** with Hg^{2+} at different concentrations in $\text{DMSO}-d_6$.

The downfield shift in $-\text{OH}$ signal and upfield shift in benzylic protons is indicative of hydrogen bonding of $-\text{OH}$ proton with counter anion/solvent molecule and coordination of the phenolic oxygen with metal ion, respectively. The aromatic protons (7.0–7.5 ppm) also demonstrate a shift of $\Delta\delta = 0.02$ – 0.08 ppm which indicates of change in the orientation of compound after interaction with Hg^{2+} ions. The complex formation between Hg^{2+} and **1** was also confirmed by ESI-MS, which indicated the formation of complex $[\mathbf{1}\cdot\text{Hg}^{2+}\cdot(\text{NO}_3^-)_2]\cdot\text{H}_2\text{O}$ (Fig. S15[†]).

Theoretical studies

In an effort to understand the binding behaviour of receptor **1** with Hg^{2+} ions, DFT calculations (B3LYP/LANL2DZ basis set on Gaussian 09 program) were performed to optimise the structure of receptor **1** and $\mathbf{1}\cdot\text{Hg}^{2+}\cdot(\text{NO}_3^-)_2$ complex (stoichiometry used was as indicated by the ESI-MS data, Fig. 9). Upon optimization, receptor **1** displayed a three-dimensional structure, where all three pods were oriented in a different direction (Fig. 9A). The orbital maps of the HOMO and LUMO of receptor **1** have been generated from the optimized geometry of receptor **1**. The orbital maps depicted that the LUMO was

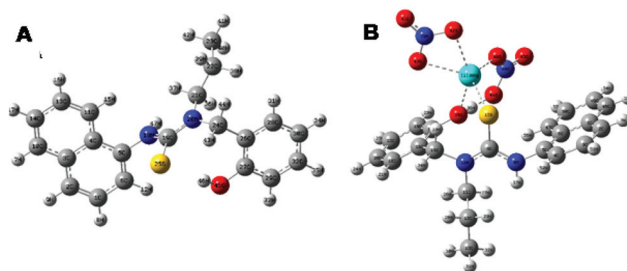


Fig. 9 The DFT optimized structure of: (A) receptor **1** and (B) $\mathbf{1}\cdot\text{Hg}^{2+}$ complex calculated at the B3LYP/LANL2DZ level. The red, blue, gray and sea green spheres refer to O, N, C, and Hg^{2+} atoms respectively.

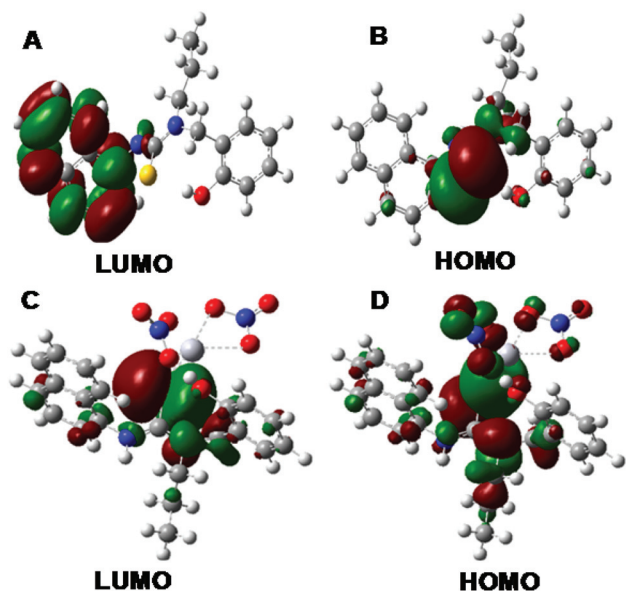


Fig. 10 A pictorial representation of HOMO–LUMO of **1** (A and B) and **1**·Hg²⁺ (C and D) calculated at the B3LYP/LANL2DZ level. The red color represents the high charge density region.

mainly centred on the naphthyl ring while the HOMO was focused on the C=S group (Fig. 10A & B). The positions of HOMO and LUMO have shown that the low fluorescence intensity of the ligand irrespective of the presence of a naphthyl fluorophore was due to the initiation of the PET process on excitation. The orbital maps of the **1**·Hg²⁺ complex clearly show the shift of HOMO–LUMO from C=S, naphthyl moiety in case of receptor **1**, to the periphery around the metal centre in the case of **1**·Hg²⁺ complex (Fig. 10C & D). This shift in orbitals led to the cancellation of the PET process that was responsible for enhancement in the fluorescent intensity of receptor **1** on addition of Hg²⁺ ions.

Analysis of water samples using the present probe (**1**) and inductively coupled plasma mass spectrometry (ICP-MS)

To evaluate the real practical application of nano-aggregates **N1**, the concentration of Hg²⁺ was analysed in environmental water samples taken from tap, lake and river water. The initial ICP-mass spectroscopy studies of the samples showed the presence of less than 0.03 μg L⁻¹ content of Hg²⁺ in the water samples. Therefore, water samples spiked with Hg²⁺ were analysed for Hg²⁺ content using the nano-aggregates **N1** in aqueous medium and ICP-MS. The river and lake water samples were first centrifuged and then filtered before performing any analysis. The analysis results obtained by using the nano-aggregates **N1** and by ICP-MS are summarized in Table 1. The results show good agreement of spiked Hg²⁺ content observed and values determined by ICP-MS. The results revealed that the present probe (**N1**) can work well in environmental samples.

Table 1 A comparison of results obtained for spiked Hg²⁺ in water samples using proposed probe and ICP-MS

Sample code	Hg ²⁺ (ng mL ⁻¹) added	Nano-aggregates N1 (mean ^a)	ICP-MS (mean ^a)
Tap water 1	10	11.3	10.9
Tap water 2	20	19.2	19.5
Tap water 3	50	51.1	50.8
Tap water 4	100	102.1	98.5
River water 1	10	11.0	11.1
River water 2	20	21.6	21.1
River water 3	50	50.9	50.6
River water 4	100	103.6	104.5
Lake water 1	10	11.5	11.3
Lake water 2	20	22.2	21.8
Lake water 3	50	51.8	52.0
Lake water 4	100	102.5	103.6

^a Mean of three determinations.

Conclusions

Two new tripodal receptors **1** and **2** have been synthesized and characterized with spectroscopy techniques (FT IR, NMR and ESI-MS). Nano-aggregates (**N1** and **N2**) of the receptors have been prepared and utilized as chemosensors in aqueous medium. Out of these, nano-aggregates **N1** can selectively recognize Hg²⁺ in aqueous medium. The interaction of Hg²⁺ with receptor is decided and supported by ¹H NMR titration, mass spectroscopy and theoretical studies. Nano-aggregates **N1** can detect the Hg²⁺ ions up to 2.4 nM level. Moreover, the nano-aggregates **N1** provide a suitable opportunity for the detection of Hg²⁺ in almost pure water, which makes their utility in environmental samples.

Experimental

General information

All chemicals used were of analytical grade and were purchased from Sigma-Aldrich Co. Elemental analyses were carried out on a Fisons instrument (Model EA 1108 CHNO). ¹H and ¹³C NMR spectra were recorded on Avance-II (Bruker) instrument, which operated at 400 MHz for ¹H NMR and 100 MHz for ¹³C NMR (chemical shifts are expressed in ppm). The absorption spectra were recorded on a Specord 250 Plus Analytik Jena spectrophotometer. The fluorescence measurements were performed on a Perkin Elmer LS55 Fluorescence spectrophotometer. The morphology analysis was carried out on scanning electron microscope (SEM JEOL JSM-6610LV) using voltage of 15 kV. The particle size of nano-aggregates was determined with dynamic light scattering (DLS) using external probe feature of Metrohm Microtrac Ultra Nanotracer Particle Size Analyzer. Agilent 7700 Series ICP-mass spectrometer was used for the determination of mercury content in water samples. The ICP-MS instrument was equipped with ASX-500 series ICP-MS auto-sampler.

Syntheses of compounds

Compound 1. *n*-Propylamine (0.77 mL, 9 mmol) was added to the solution of 2-hydroxy benzaldehyde (1 mL, 9 mmol) in 10 mL of MeOH and stirred overnight at room temperature. The solid product (**1a**, Schiff base) obtained was filtered and dried in air. The Schiff base, **1a** was then dissolved in 50 mL of MeOH-THF (1:1, v/v) and was reduced with NaBH₄ (1.5 mg, 36 mmol). The reaction mixture was allowed to stir at room temperature overnight and the solvent was removed under reduced pressure. The residue obtained was dissolved in CHCl₃ and extracted with water. The extracted organic layers were dried over Na₂SO₄ and concentrated to afford reduced amine **1b**. The compound **1b** was dissolved in CHCl₃ (15 mL) and refluxed with 1-naphthyl isothiocyanate (0.310 g, 2 mmol) at 60 °C for 4 hours and then stirred overnight at room temperature. The solvent was removed under reduced pressure and solid residue was recrystallized in MeOH to obtain pure compound **1** in 92% yield. FT IR (KBr) (ν_{\max} , cm⁻¹): 3365(br), 3252(w), 2923(m), 1589(s), 1515(s); ¹H NMR (400 MHz, DMSO-d₆) δ : 9.76(br, 1H, NH), 9.38 (s, 1H, OH), 7.93 (d, 1H, *J* = 6.8 Hz, ArH), 7.84–7.77 (m, 2H, ArH), 7.51–7.48 (m, 3H, ArH), 7.32(d, 1H, *J* = 7.2 Hz, ArH), 7.23 (d, 1H, *J* = 7.4 Hz, ArH), 7.14(t, 1H, *J* = 7.9 Hz, ArH), 6.90–6.86(m, 2H, ArH), 5.06 (s, 2H, CH₂), 3.70 (t, 2H, *J* = 7.5 Hz, CH₂), 1.73–1.71 (m, 2H, CH₂), 0.89 (t, 3H, *J* = 7.2 Hz, CH₃); ¹³C NMR (100 MHz, DMSO-d₆) δ : 181.9, 156.3, 135.4, 134.4, 131.8, 130.4, 128.7, 128.2, 127.5, 127.3, 127.0, 126.5, 126.2, 125.6, 122.5, 119.8, 117.4, 53.7, 50.2, 20.2, 11.6; ESI-MS *m/z* = 351.2 [M + H]⁺; CHN analysis calcd for (C₂₁H₂₂N₂OS): C, 71.97; H, 6.33; N, 7.99; found: C, 71.63; H, 6.28; N, 7.85.

Compound 2. *n*-Propylamine (0.82 mL, 10 mmol) was added to a solution of 4-hydroxy benzaldehyde (1.2 g, 10 mmol) in 10 mL of MeOH and stirred overnight at room temperature. The solid product (**2a**, Schiff base) obtained was filtered and dried in air. The Schiff base, **2a** was then dissolved in 50 mL of MeOH-THF (1:1, v/v) and was reduced with NaBH₄ (1.57 mg, 40 mmol). The reaction mixture was allowed to stir overnight at room temperature and the solvent was removed under reduced pressure. The residue so obtained was dissolved in CHCl₃ and extracted with water. The extracted organic layers were dried over Na₂SO₄ and concentrated to afford reduced amine **2b**. Compound **2b** was dissolved in CHCl₃ (15 mL) and refluxed with 1-naphthyl isothiocyanate (0.227, 1.23 mmol) at 60 °C for 4 hours and then stirred at room temperature overnight. The solvent was removed under reduced pressure and the solid residue was recrystallized in MeOH to obtain pure compound **2** in 64% yield. FT IR (KBr) (ν_{\max} , cm⁻¹): 3112(w), 2926(w), 1583(s), 1516(s); ¹H NMR (400 MHz, CDCl₃) δ : 7.79 (d, 1H, *J* = 8.1 Hz, ArH), 7.72 (d, 1H, *J* = 7.6 Hz, ArH), 7.50–7.37 (m, 5H, ArH), 7.26–7.27 (m, 1H, ArH), 6.86 (d, 2H, *J* = 6.2 Hz, ArH), 6.78 (d, 1H, *J* = 8.1 Hz, ArH), 4.9(s, 2H, CH₂), 3.83 (q, 2H, *J* = 7.7 Hz, CH₂), 1.82 (m, 2H, CH₂), 0.96 (t, 3H, *J* = 7.4 Hz, CH₃); ¹³C NMR (100 MHz, CDCl₃) δ : 183.3, 157.1, 137.5, 135.8, 134.3, 130.6, 130.3, 128.6, 127.5, 126.7, 126.2, 125.7, 125.5, 122.4, 118.8, 115.5, 113.7,

54.6, 20.9, 11.5; ESI-MS *m/z* = 351.2 [M + H]⁺; CHN analysis calcd for (C₂₁H₂₂N₂OS): C, 71.97; H, 6.33; N, 7.99; found: C, 71.53; H, 6.30; N, 7.93.

Syntheses of nano-aggregates N1 and N2

The nano-aggregates were synthesized by a re-precipitation method.³⁴ A solution of the respective compound (1 mM) in acetonitrile was prepared. 1 mL of the working solution was slowly injected into 100 mL of water with a micro-syringe. The solution is then sonicated for a total of 10 minutes, making sure the temperature of the solution containing nanoparticles did not rise above 10 °C.

Recognition studies

The recognition studies were performed at 25 ± 1 °C, and the solutions were shaken for a sufficient time before recording the spectrum. The binding ability of nano-aggregates **N1–2** (10 μM) in aqueous medium was determined by adding 50 μM of a metal nitrate/tetrabutylammonium salt of anions to 5 mL solution of **N1–2** taken in volumetric flasks. The volumetric flasks were allowed to stand for 30 minutes before the spectra were recorded. For Hg²⁺ titrations, Hg(NO₃)₂ was added to volumetric flasks containing nano-aggregate solutions of **N1–2** in aqueous medium. To evaluate any possible interference due to different cations for the estimation of Hg²⁺, solutions were prepared containing **N1–2** (10 μM) with and without other interfering metal ions (50 μM). The effect of ionic strength was explored by recording the spectra at different concentrations of tetrabutylammonium nitrate (0–200 equivalent). pH titrations were performed to understand the effect of pH on the recognition profile of **N1** and **N2**.

Acknowledgements

This work was supported with a research grant (SR/FT/CS-97/2010(G)) from the Department of Science and Technology (DST), Government of India. S. K. acknowledges DST for an INSPIRE fellowship.

Notes and references

- 1 M. Alfonso, A. Tarraga and P. Molina, *Inorg. Chem.*, 2013, **52**, 7487.
- 2 J. Zhang, Y. Zhou, W. Hu, L. Zhang, Q. Huang and T. Ma, *Sens. Actuators, B*, 2013, **183**, 290–296.
- 3 S. Lee, C.-H. Chen and A. H. Flood, *Nat. Chem.*, 2013, **5**, 704–710.
- 4 Y. Hong, S. Chen, C. Wai, T. Leung, J. Wing, Y. Lam, J. Liu, N.-W. Tseng, R. T. K. Kwok, Y. Yu, Z. Wang and B. Z. Tang, *ACS Appl. Mater. Interfaces*, 2011, **3**, 3411–3418.
- 5 J.-H. Ye, L. Duan, C. Yan, W. Zhang and W. He, *Tetrahedron Lett.*, 2012, **53**, 593–596.
- 6 H.-W. Li, B. Wang, Y.-Q. Dang, L. Li and Y. Wu, *Sens. Actuators, B*, 2010, **148**, 49–53.

- 7 A. Yari and F. Papi, *Sens. Actuators, B*, 2011, **160**, 698–704.
- 8 X. Cheng, S. Li, A. Zhong, J. Qin and Z. Li, *Sens. Actuators, B*, 2011, **157**, 57–63.
- 9 K. Farhadi, M. Forough, R. Molaei, S. Hajizadeh and A. Rafipour, *Sens. Actuators, B*, 2012, **161**, 880–885.
- 10 W. F. Fitzgerald, C. H. Lamborg and C. R. Hammerschmidt, *Chem. Rev.*, 2007, **107**, 641–662.
- 11 J. S. Lee, M. S. Han and C. A. Mirkin, *Angew. Chem. Int. Ed.*, 2007, **119**, 4171–4174.
- 12 H. H. Harris, I. J. Pickering and G. N. George, *Science*, 2003, **301**, 1203–1203.
- 13 P. B. Tchounwou, W. K. Ayensu, N. Ninashvili and D. Sutton, *Environ. Toxicol.*, 2003, **18**, 149–175.
- 14 F. Wang, S. W. Nam, Z. Q. Guo, S. S. Park and J. Y. Yoon, *Sens. Actuators, B*, 2012, **161**, 948–953.
- 15 N. Wanichacheva, K. Setthakarn, N. Prapawattanapol, O. Hanmeng, V. S. Lee and K. Grudpan, *J. Lumin.*, 2012, **132**, 35–40.
- 16 Y. L. Liu, X. Lv, Y. Zhao, M. L. Chen, J. Liu, P. Wang and W. Guo, *Dyes Pigm.*, 2012, **92**, 909–915.
- 17 V. Bhalla, Roopa, M. Kumar, P. R. Sharma and T. Kaur, *Inorg. Chem.*, 2012, **51**, 2150–2156.
- 18 X.-Q. Zhan, Z.-H. Qian, H. Zheng, B.-Y. Su, Z. Lan and J.-G. Xu, *Chem. Commun.*, 2008, 1859–1861.
- 19 J. Wen, Z. Geng, Y. Yin and Z. Wang, *Dalton Trans.*, 2011, **40**, 9737–9745.
- 20 Y. Zhou, C.-Y. Zhu, X.-S. Gao, X.-Y. You and C. Yao, *Org. Lett.*, 2010, **12**, 2566–2569.
- 21 X. Liu, X. Shu, X. Zhou, X. Zhang and J. Zhu, *J. Phys. Chem. A*, 2010, **114**, 13370–13375.
- 22 D. Homraruén, T. Sirijindalert, L. Dubas, M. Sukwattanasinitt and A. Ajavakom, *Tetrahedron*, 2013, **69**, 1617–1621.
- 23 H.-F. Wang and S.-P. Wu, *Tetrahedron*, 2013, **69**, 1965–1969.
- 24 K. M. Shafeekh, M. K. A. Rahim, M. C. Basheer, C. H. Suresh and S. Das, *Dyes Pigm.*, 2013, **96**, 714–721.
- 25 D. P. Murale, H. Liew, Y.-H. Suh and D. G. Churchill, *Anal. Methods*, 2013, **5**, 2650–2652.
- 26 A. P. Singh, D. P. Murale, Y. Ha, H. Liew, K. M. Lee, A. Segev, Y.-H. Suh and D. G. Churchill, *Dalton Trans.*, 2013, **42**, 3285–3290.
- 27 K. Kim, S. H. Choi, J. Jeon, H. Lee, J. O. Huh, J. Yoo, J. T. Kim, C.-H. Lee, Y. S. Lee and D. G. Churchill, *Inorg. Chem.*, 2011, **50**, 5351–5360.
- 28 S. H. Choi, K. Pang, K. Kim and D. G. Churchill, *Inorg. Chem.*, 2007, **46**, 10564–10577.
- 29 Y. Hong, J. W. Y. Lama and B. Z. Tang, *Chem. Soc. Rev.*, 2011, **40**, 5361–5388.
- 30 K. Shiraishi, T. Sanji and M. Tanaka, *Tetrahedron Lett.*, 2010, **51**, 6331–6333.
- 31 Y. Liu, Y. Tang, N. N. Barashkov, I. S. Irgibaeva, J. W. Y. Lam, R. Hu, D. Birimzhanova, Y. Yu and B. Z. Tang, *J. Am. Chem. Soc.*, 2010, **132**, 13951–13953.
- 32 C. Park and J.-I. Hong, *Tetrahedron Lett.*, 2010, **51**, 1960–1962.
- 33 Y. Hong, J. W. Y. Lam and B. Z. Tang, *Chem. Commun.*, 2009, 4332–4353.
- 34 R. O. Al-Kaysi, A. M. Müller, T. S. Ahn, S. Lee and C. J. Bardeen, *Langmuir*, 2005, **21**, 7990–7994.
- 35 S. Yagai, Y. Goto, X. Lin, T. Karatsu, A. Kitamura, D. Kuzuhara, H. Yamada, Y. Kikkawa, A. Saeki and S. Seki, *Angew. Chem., Int. Ed.*, 2012, **51**, 6643–6647.
- 36 Q. Zeng, Z. Li, Y. Dong, C. Di, A. Qin, Y. Hong, L. Ji, Z. Zhu, C. K. W. Jim, G. Yu, Q. Li, Z. Li, Y. Liu, J. Qin and B. Z. Tang, *Chem. Commun.*, 2007, 70–72.
- 37 S. Kim, H. E. Pudavar, A. Bonoiu and P. N. Prasad, *Adv. Mater.*, 2007, **19**, 3791–3795.
- 38 A. P. De Silva, H. Q. N. Gunaratne, T. Gunnlaugsson, A. J. M. Huxley, C. P. McCoy, J. T. Rademacher and T. E. Rice, *Chem. Rev.*, 1997, **97**, 1515–1566.
- 39 M. Zhu, M. Yuan, X. Liu, J. Xu, J. Lv, C. Huang, H. Liu, Y. Li, S. Wang and D. Zhu, *Org. Lett.*, 2008, **10**, 1481–1484.